Preprint typeset using LaTeX style emulateapj v. 11/12/01

3D SIMULATIONS OF RELATIVISTIC PRECESSING JETS PROBING THE STRUCTURE OF SUPERLUMINAL SOURCES

Miguel Ángel Aloy[1], José María Martí[2], José Luís Gómez[3,4], Iván Agudo[3], Ewald Müller[1], José María Ibáñez[2]

Draft version February 7, 2003

ABSTRACT

We present the results of a three-dimensional, relativistic, hydrodynamic simulation of a precessing jet into which a compact blob of matter is injected. A comparison of synthetic radio maps computed from the hydrodynamic model, taking into account the appropriate light travel time delays, with those obtained from observations of actual superluminal sources shows that the variability of the jet emission is the result of a complex combination of phase motions, viewing angle selection effects, and non-linear interactions between perturbations and the underlying jet and/or the external medium. These results question the hydrodynamic properties inferred from observed apparent motions and radio structures, and reveal that shock-in-jet models may be overly simplistic.

Subject headings: galaxies: jets – hydrodynamics – radiation mechanisms: non-thermal

1. INTRODUCTION

Numerical hydrodynamic simulations were initially used to study radiosources from their largest scales (Burns, Norman, & Clarke 1991) to the collimation and formation of their associated jets (Koide et al. 2002). Due to the relativistic nature of these sources, *relativistic* hydrodynamic simulations have become necessary to study the superluminal sources present in the nuclei of active galaxies and in the microquasars of our galaxy. Improving on previous idealized analytical calculations (Marscher & Gear 1985), these numerical methods are capable of studying the time–dependent non–linear relativistic fluid dynamics, like for instance the formation and propagation of shocks (Martí, Müller, & Ibáñez 1994; Duncan & Hughes 1994; Koide, Nishikawa, & Mutel 1996; Falle & Komissarov 1996; Aloy et al. 1999a). The computation of the non-thermal emission from such hydrodynamic models provides the means for a direct comparison between observations and theory, and is hence a significant step forward towards an understanding of the emission and structural variability of relativistic jets (Gómez et al. 1995, 1997; Komissarov & Falle 1997; Mioduszewski, Hughes, & Duncan 1997; Aloy et al. 1999b, 2000; Agudo et al. 2001).

Motivated by recent observations (**?**, e.g.,)]JL00,Ti01,We01 revealing complex jet structure and dynamics suggestive of being the result of multi–dimensional non–linear jet instabilities, we present a three–dimensional relativistic hydrodynamic and emission simulation of a precessing jet.

2. HYDRODYNAMIC MODEL

Our hydrodynamic code GENESIS (Aloy et al. 1999a) is based on high resolution shock capturing techniques, best suited to describe ultra-relativistic flows with strong discontinuities. The code employs the method of lines to achieve third order accuracy both in space (using a Parabolic Piecewise Monotonic -PPM- inter-cell reconstruction) and time (by means of a third order Total Variation Diminishing -TVD- Runge-Kutta scheme). Guided by observational data we simulate a jet composed of an ultra-relativistic plasma (adiabatic index 4/3, and specific energy $50c^2$, c being the speed of light) in pressure equilibrium with an ambient atmosphere in which the jet propagates. The plasma is injected with a bulk Lorentz factor of 6, and is 10^3 times lighter than the environment. We enforce a twofold precession of the jet by imposing helical perturbations on the injection velocity with amplitudes ζ_1 (ζ_2) = 0.035 (0.005), and periodicities τ_1 (τ_2) = $400\,R_b/c$ ($25\,R_b/c$), where R_b is the beam radius (the definitions of $\zeta_{1,2}$ and $\tau_{1,2}$ are the same as in Aloy et al. (1999b)). The first, long wavelength precession ($\lambda_1 = 400\,R_b$) causes a slight bending of the jet (within the computational domain of longitudinal size $90\,R_b$), while the second precession, with a much shorter wavelength ($\lambda_2 = 25R_b$) and smaller amplitude than the first one, gives rise to a small helical modulation of the beam. Both structural characteristics are observed in many astrophysical sources (**?**, e.g., 3C 120;)]JL00.

According to the recent observations of Marscher et al. (2002) radio components are generated by the injection into the jet of material coming from the inner accretion disk. Motivated by these observations, we perturb the jet by injecting a blob of relativistic particles through the jet inlet during $0.8\,R_b/c$ in the frame attached to the source (LAB-frame). The blob, initially a cylindrical region of thickness $0.8\,R_b$ and width $1.0\,R_b$, is four times denser than the jet plasma, but has the same velocity and internal energy per particle. As the injected perturbation travels downstream it spreads asymmetrically along the beam and splits into two regions (Fig. 1) that have distinct observational signatures (§ 3). The fact that injected jet perturbations experience substantial evolution is general, i.e., is not specific to the perturbation that we have chosen. Indeed, a similar hydrodynamic evolution should be

[1] Max-Planck-Institut für Astrophysik, Karl-Schwarzschild-Str. 1, D-85741 Garching, Germany. maa@mpa-garching.mpg.de

[2] Departamento de Astronomía y Astrofísica, Universidad de Valencia, 46100 Burjassot (Valencia), Spain. jose-maria.marti@uv.es

[3] Instituto de Astrofísica de Andalucía, CSIC, Apartado 3004, 18080 Granada, Spain. jlgomez@iaa.es

[4] Institut d'Estudis Espacials de Catalunya/CSIC, Edifici Nexus, c/ Gran Capità, 2-4, E-08034 Barcelona, Spain

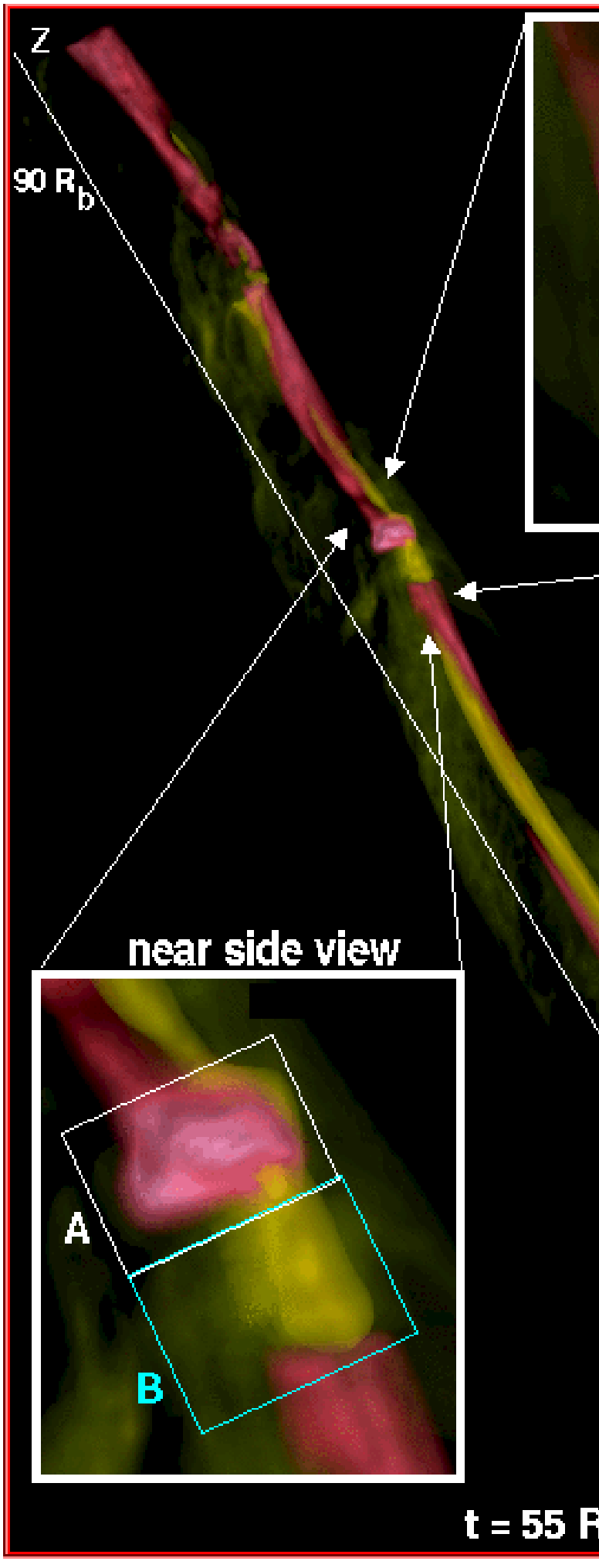
Z
90 R_b
near side view
A
B
t = 55 R

FIG. 1.— Three dimensional ray cast view of the simulated jet in the LAB-frame. The image is produced by ray tracing the Lorentz factor and the pressure, assigning an opacity to each volume element proportional to the magnitude of each variable. The computational domain is a cuboid of physical size $14 \times 14 \times 90$ beam radii covered by a uniform Cartesian (X,Y,Z) grid of 168x168x1080 zones. Those parts of the fluid having Lorentz factors larger than the bulk Lorentz factor of the beam in the injection nozzle ($W_b = 6$) show up as pink regions. Strong yellowish green colors encode the energy density times the beam mass fraction ($X = \rho_b/\rho$, ρ_b and ρ being the densities of beam and of the fluid, respectively) and diffuse greenish shades the energy density itself. In both cases, the intensity is a measure of the corresponding quantity's value (brighter meaning larger). The two insets are zooms of the perturbation, the bottom one also showing regions A and B defined in the text.

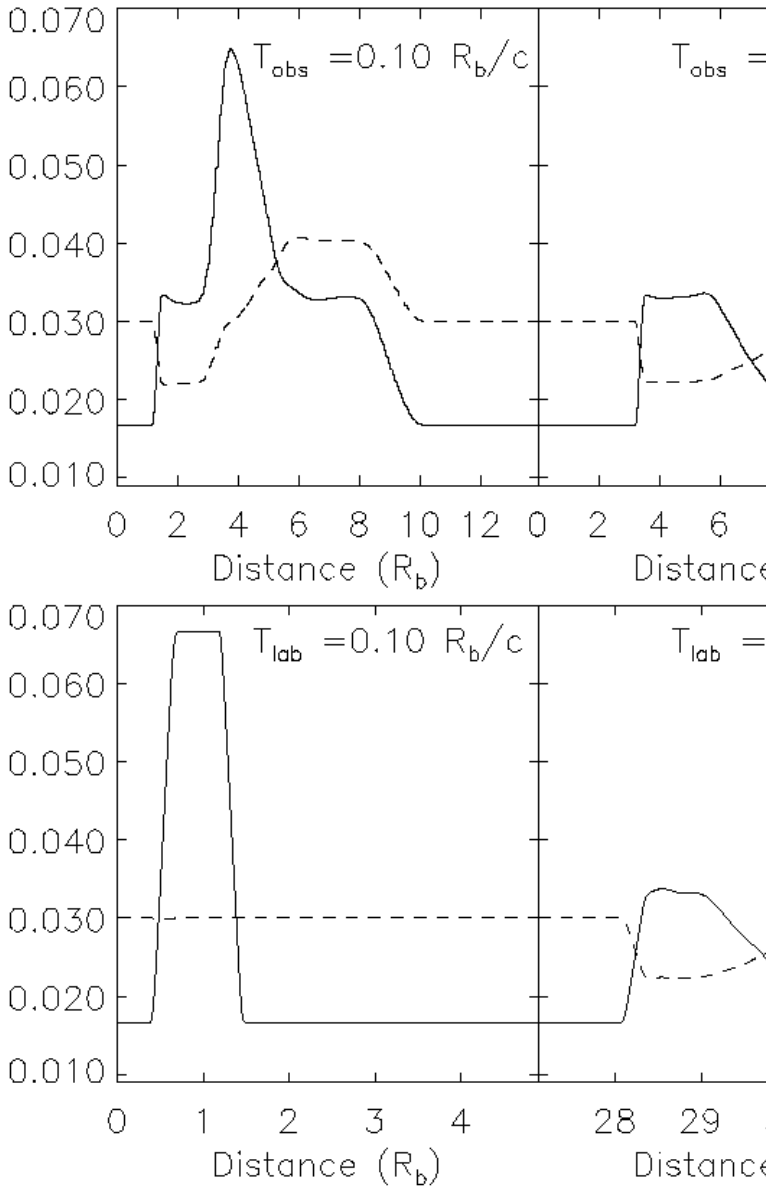

FIG. 2.— Snapshots of the 1D evolution of the energy density (solid line) and the Lorentz factor (divided by 200; dashed line) of a square component in a uniformly moving background medium as seen in the O-frame for a viewing angle of 15° (top panels) and in the LAB-frame (bottom panels). Physical parameters of both background and perturbation are the same as in the 3D simulation. The quasisteady state (rightmost panels) is very similar in both frames, but due to the time dilation effect the apparent size is much larger in the O-frame.

expected for any perturbation that either does not match the shock jump conditions at its boundaries or propagates along a non-uniform beam. An idealized 1D model of the perturbation allows us to explain the basic features of its evolution. The original state disappears after $\approx 15\,R_b/c$ and displays a noticeable split after $30\,R_b/c$ and beyond in the LAB-frame (Fig. 2). In the 3D simulation the evolution of the perturbation is also affected by its interaction with the external medium and changing beam conditions downstream. The front region (A) of the original blob shows the largest Lorentz factor (≥ 9) and relatively small energy density, while the back region (B) possesses the largest energy density but the smallest Lorentz factor (≈ 4.5).

Initially the perturbation is ballistic as a consequence of its high relativistic density (≈ 9.7 times that of the external medium) and moves in a straight trajectory until it impacts on the bent walls of the beam, between times 20 and $40\,R_b/c$. This causes an increase of the internal energy density and a reduction of the Lorentz factor in the region of maximum shear (Fig. 3b, 3c). The heating is a consequence of the compression of the perturbation, which is enhanced by the presence of a standing shock in the beam (Fig. 3a). The interaction also leads to the formation of a conical shaped bow shock that continues along with the perturbation expanding at $\sim 0.2\,c$, which is seen in Fig. 3a as a strong increase of the energy density emerging from the component and forming a small angle with the beam. In the bottom part of the component the bow shock is weaker. The effect of the collision against the edge of the beam is relatively small because of the very

small impact angle of $\sim 5°$. A 2D analytic modeling of the impact shows the generation of a rarefaction instead of a shock for impact angles smaller than $\sim 35°$. [This is a genuine relativistic effect (Pons, Martí, & Müller 2000; Rezolla & Zanotti 2002).] After $\sim 55\,R_b/c$ the perturbation is no longer ballistic and no longer covers the whole beam's width.

3. EMISSION

We compute the synchrotron emission from the hydrodynamic model assuming that the magnetic energy density is proportional to the particle energy density and that this proportionality remains constant throughout the whole computational domain (**?**, as in)]JL95. We also assume that magnetic field is dynamically negligible and we account for the appropriate relativistic effects (**?**, including light travel time delays as in)]JL97, aimed to obtain synthetic radio maps (Fig. 4) that can be compared with observations of superluminal sources. To relate emission features in the observer's frame (O-frame; Fig. 4) with their hydrodynamic counterparts, we provide a space-time diagram (Fig. 5).

FIG. 3.— Longitudinal slice through part of the jet showing the logarithm of the energy density, e, (in arbitrary units) when the perturbation passes through the first recollimation shock (a). The bottom panels show the logarithm of the energy density (b; with the same scale as the panel a) and the bulk Lorentz factor, W, (c) for a transverse slice at z=11.5 R_b (vertical white line in panel a). In all the panels the white lines are isocontours of beam mass fraction (see caption of Fig. 1) 0.5 roughly separating the beam from the external medium, the vertical axis provides the scale in R_b, and the crosses mark the position of the jet axis if it were axisymmetric. The spiral structure present in the ambient medium (b) is caused by the precession of the jet.

Figure 4 shows the appearance of a large region of increased emission, associated with the imposed perturbation, passing by several standing knots (S1, S2, S3) caused by jet recollimation shocks. The large extension of this new emitting region is caused by the light travel time delays between the front and back of the perturbation, which stretch it by a factor $(1-\beta\cos\theta)^{-1}$ (β and θ being the velocity –in units of c– of propagation and the viewing angle, respectively). As a consequence, the structure of the perturbation is magnified leading to brightness distribution variations within the component in the O-frame. This may have significant implications when interpreting the observations of superluminal sources. First of all, the quite common practice of identifying brightness peaks in radio maps with components may be misleading, as the component selected in this way may only be one of many brightness features caused by a single perturbation and may not be related to any physical structure on its own. Moreover, a component may result from different regions of the perturbation having different hydrodynamic proper-

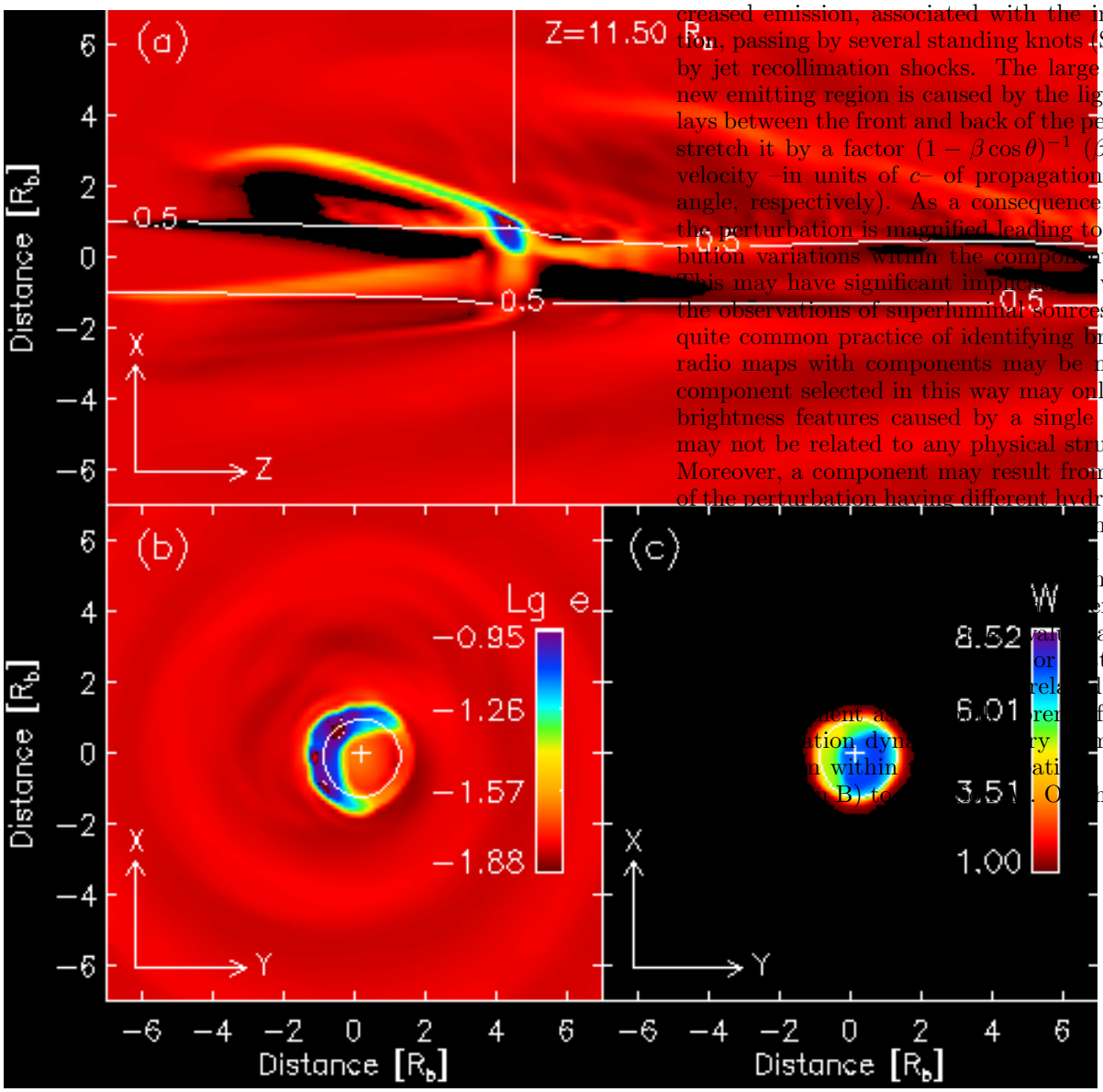

ne brightness peak Fig. 4 as compo- nt motion from 1.4 ntz factors of the are 2 to 4.3, which ttern speeds in the l to the motion of factors (Fig. 2) in n the initial value to values ranging he other hand, the

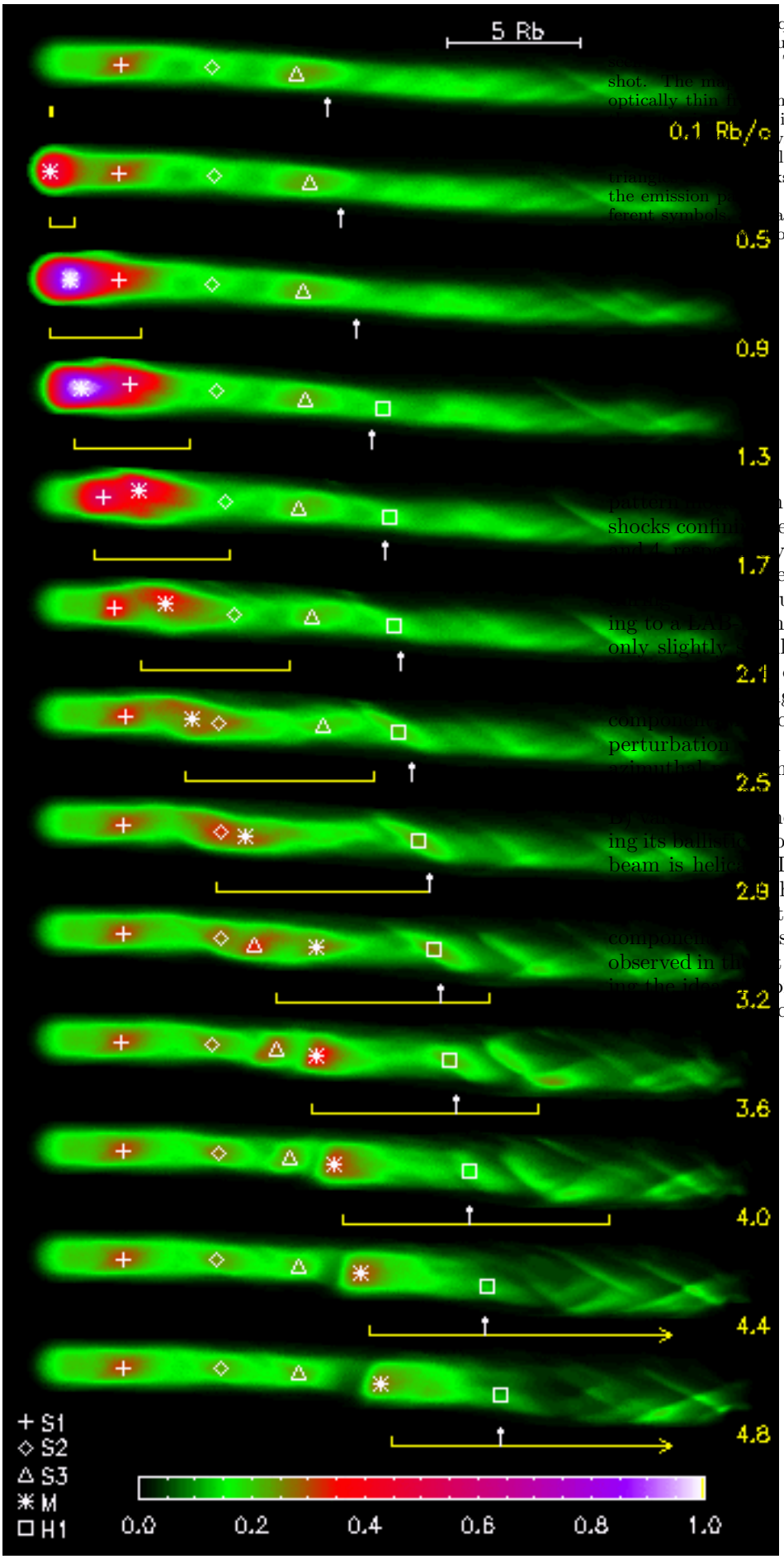

quence of the simulated radio maps (total in-
nits using a square root brightness scale) as
The epoch is shown at the right of each snap-
computed for a viewing angle of 15° and an
ncy of 22 GHz. Yellow underbrackets indicate
imposed hydrodynamic perturbation (For the
s indicate that the front of the perturbation is
left and right bounds are associated to the red
s in the inset of Fig. 5, respectively. Knots in
(S1, S2, S3, M and H1) are marked with dif-
a white arrow gives the position of component
om Fig. 5.

the perturbation that correspond to the
egions A and B have Lorentz factors of 7
, which differ significantly from the esti-
e proper motion of M is almost constant
ur epochs and equals $1.7\,c$, correspond-
e pattern Lorentz factor of 2.2, which is
ler than the Lorentz factor of the back
during these epochs (≈ 2.7; Fig. 5).
ghtness distribution of the superluminal
o changes due to the interaction of the
the ambient medium and the jet. The
n of the region of maximum interaction
the maximum energy density in region
e because the perturbation moves (dur-
och) along a straight trajectory while the
The resulting interaction, together with
he perturbation when it passes through
the jet, leads to transverse motions of the
sion peak. A similar behavior has been
of 3C 120 (Gómez et al. 2001), support-
precessing jet in this source and of inter-
omponents and the external medium.

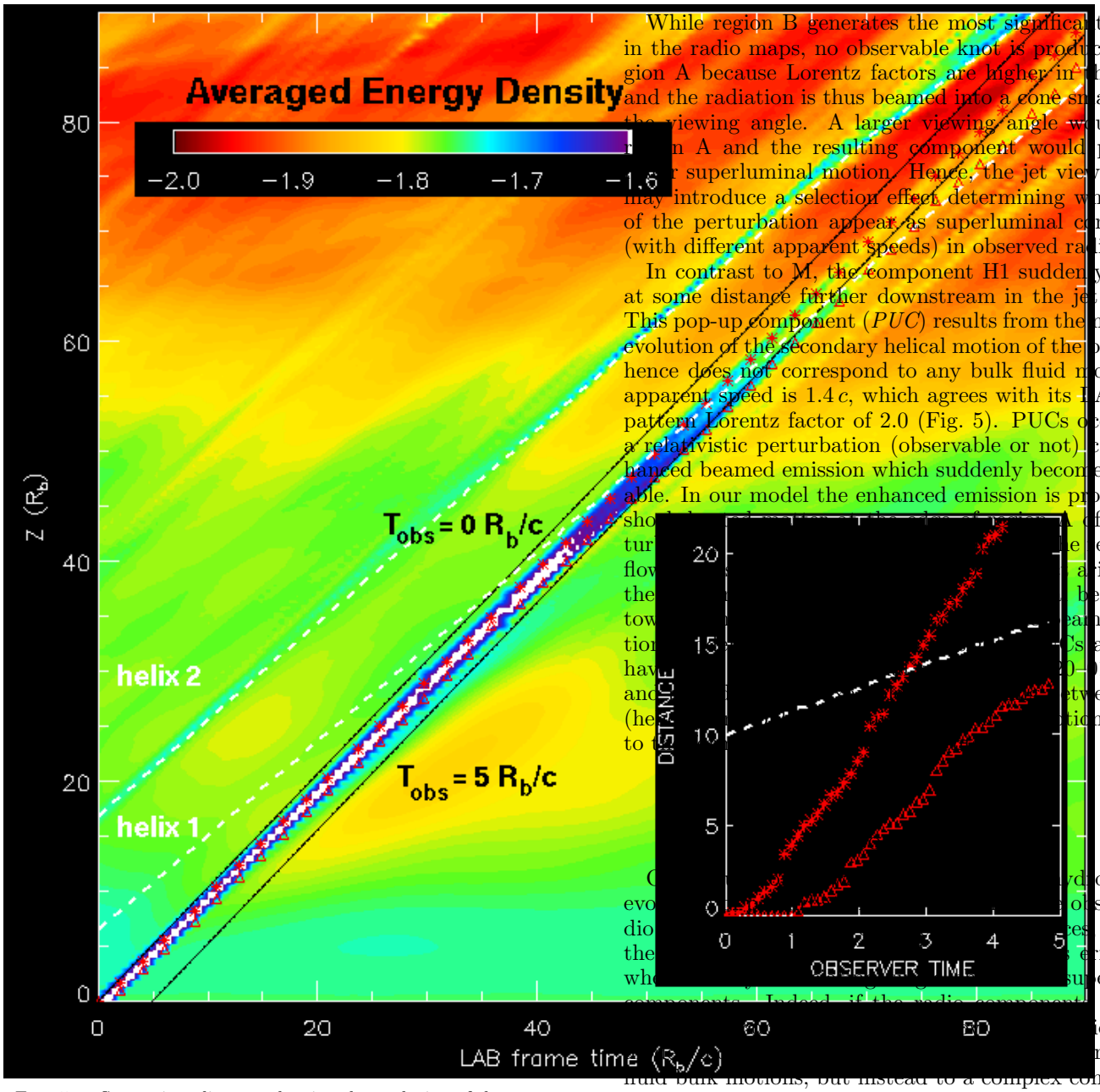

FIG. 5.— Space-time diagram showing the evolution of the energy density along the jet. Every vertical pixel line is a snapshot of the jet's longitudinal structure averaged across azimuthal slices. The trajectories of two "elbows" (i.e., local bends of the helix that have evolved non-linearly and form kinks in the beam where the energy density and the density are large and leave a trace in the space-time diagram and in the radio maps of Fig. 4) of the secondary helix (helix 1 and helix 2; white dashed lines) of the helical jet propagate with pattern Lorentz factors between 2.0-2.6. The perturbation has average bulk Lorentz factors of 3.7 and 7.1 for the back (B) and front (A) regions, respectively. The back shock of region B decelerates between 40 and 55 R_b/c reducing its pattern Lorentz factor to 2.7. The area between the two black lines (isocrones in the O-frame corresponding to times $0R_b/c$ and $5R_b/c$) covers the whole time evolution of Fig. 4. The propagation of the component H1 (= helix 1) and of the main perturbation (red asterisks: front shock of region A; red triangles: back shock of region B) are illustrated both in the LAB- and in the O-frame (inset).

While region B generates the most significant features in the radio maps, no observable knot is produced by region A because Lorentz factors are higher in this region and the radiation is thus beamed into a cone smaller than the viewing angle. A larger viewing angle would beam [illegible] A and the resulting component would present a [illegible] superluminal motion. Hence, the jet viewing angle may introduce a selection effect determining which parts of the perturbation appear as superluminal components (with different apparent speeds) in observed radio maps.

In contrast to M, the component H1 suddenly appears at some distance further downstream in the jet (Fig. 4). This pop-up component (*PUC*) results from the non-linear evolution of the secondary helical motion of the beam, and hence does not correspond to any bulk fluid motion. Its apparent speed is $1.4\,c$, which agrees with its LAB-frame pattern Lorentz factor of 2.0 (Fig. 5). PUCs occur when a relativistic perturbation (observable or not) causes enhanced beamed emission which suddenly becomes observable. In our model the enhanced emission is produced by sho[illegible] of the perturbation [illegible] relativistic flow [illegible] arises when the [illegible] beam turns tow[illegible] ened radiation [illegible] C's appear to hav[illegible] 14;)]Zh00 and [illegible] tween phase (he[illegible] tions leading to [illegible]

C[illegible] ydrodynamic evo[illegible] served radio [illegible] and that the[illegible] error-prone wh[illegible] perluminal [illegible] of actual [illegible] ied in our [illegible] related to fluid bulk motions, but instead to a complex combination of bulk and phase motions, viewing angle selection effects, and non-linear interactions between perturbations and the underlying jet and/or ambient medium. Further simulations spanning a wide range of the relevant parameters are underway.

M. A. A. acknowledges the EU-Commission for a fellowship (MCFI-2000-00504). This research was supported in part by the Spanish Dirección General de Enseanza Superior grant AYA-2001-3490 and through an agreement between the Max-Planck-Gesellschaft and the Consejo Superior de Investigaciones Científicas.

REFERENCES

Agudo, I., Gómez, J. L., Martí, J. M., Ibáñez, J. M., Marscher, A. P., Alberdi, A., Aloy, M. A., & Hardee, P. E. 2001, ApJ, 549, L183
Aloy, M. A., Gómez, J. L., Ibáñez, J. M., Martí, J. M., & Müller, E. 2000, ApJ, 528, L85
Aloy, M. A., Ibáñez, J. M., Martí, J. M., Gómez, J. L., & Müller, E. 1999b, ApJ, 523, L125
Aloy, M. A., Ibáñez, J. M., Martí, J. M., & Müller, E. 1999a, ApJS, 122, 151
Burns, J. O., Norman, M. L., & Clarke, D. A. 1991, Science, 253, 522
Duncan, G. C., & Hughes, P. A. 1994, ApJ, 436, L119
Falle, S. A. E. G., & Komissarov, S. S. 1996, MNRAS, 278, 586
Gómez, J. L., Marscher, A. P, Alberdi, A., Jorstad, S. G., & Agudo, I. 2001, ApJ, 561, L161
Gómez, J. L., Marscher, A. P, Alberdi, A., Jorstad, S. G., & García-Miró, C. 2000, Science, 289, 2317
Gómez, J. L., Martí, J. M., Marscher, A. P., Ibáñez, J. M., & Alberdi, A. 1997, ApJ, 482, L33
Gómez, J. L., Martí, J. M., Marscher, A. P., Ibáñez, J. M., & Marcaide, J. M. 1995, ApJ, 449, L19
Koide, S., Nishikawa, K., & Mutel, R. L. 1996, ApJ, 463, L71
Koide, S., Shibata, K., Kudoh, T., & Meier, D. 2002, Science, 295, 1688
Komissarov, S. S., & Falle, S. A. E. G. 1997, MNRAS, 288, 833
Marscher, A. P. & Gear, W. K. 1985, ApJ, 298, 114
Marscher, A. P., Jorstad, S. G., Gómez, J. L., Aller, M. F., Teräsranta, H., Lister, M. L., & Stirling, A. M. 2002, Nature, 417, 625
Martí, J. M., Müller, E., & Ibáñez, J. M. 1994, A&A, 281, L9
Mioduszewski, A. J., Hughes, P. A., & Duncan, G. C. 1997, ApJ, 476, 649
Pons, J. A., Martí, J. M., & Müller, E. 2000, J. Fluid Mech., 422, 125
Rezolla, L., & Zanotti, O. 2002, PRL, 89, 114, 501
Tingay S. J., Preston R. A., & Jauncey D. L. 2001, AJ, 122, 1697
Wehrle, A. E., Piner, B. G., Unwin, S. C., Zook, A. C., Xu, W., Marscher, A. P., Teräsranta, H., & Valtaoja, E. 2001, ApJS, 133, 297
Zhou, J. F., Hong, X. Y., Jiang, D. R., & Venturi, T. 2000, ApJ, 541, L13